INTERNATIONAL JOURNAL OF
COASTAL, OFFSHORE & ENVIRONMENTAL ENGINEERING IJCOE Vol.1 •/No. 4/ Autumn 2025 (35-45)

Available online at: www. Ijcoe.org

Numerical Simulation of Plate Scour Around Offshore Platforms and Strategies to Prevent it

Seyed Amirhosein Mirabotalebi[1], Mehdi Nezhadnaderi[2]* and Reza Zahedi [3] Mohammad Gholami[4], Taha Mehrzad[5] andAli Sheykhbahaei[6]

[1)] Department of Civil Engineering, To.C., Islamic Azad University, Tonekabon, Iran. 2270123301@gmail.com
[*2)] Department of Civil Engineering, To.C., Islamic Azad University, Tonekabon, Iran. (Corresponding Author).
*mehdi.nezhadnaderi@iau.ac.ir
[3)] Department of Civil Engineering, To.C., Islamic Azad University, Tonekabon, Iran.
2219185427@iau.ir
[4)] Department of Civil Engineering, Tonekabon Branch, Islamic Azad University, Tonekabon,
2092366262@iau.ir
[5)]Department of Civil Engineering, To.C., Islamic Azad University, Tonekabon, Iran.
22701499114@iau.ir
[6)] PhD Candidate in Physical Oceanography at university of Hormozgan/ Iranian National Institute for Oceanography and Atomospheric science, Ali.sheykhbahaei@inio.ac.ir
*mehdi.nezhadnaderi@iau.ac.ir (*Corresponding author's email)

ARTICLE INFO

Article History:
Received: 25 MAY 2025
Accepted: 20 JAN 2026

Keywords:
Offshore platform baselines, flow patterns, scouring, barrier plates, pressure gradient.

ABSTRACT

With the increase in construction in the sea, protective structures are considered to prevent their instability in the marine environment. Among the coastal protective structures, submerged plates are used in marine structural engineering to prevent scour. Therefore, it is very important to study and understand the erosion and sedimentation process in the area of the offshore platform base lines in terms of design, protection and maintenance. In this research, using the computational fluid dynamics method and Fluent software, the flow around the submerged offshore platform base was simulated with different Reynolds number states. The results of the iso velocity lines, m/s, show that the speed decreases behind the offshore platform base. The maximum speed is below the offshore platform base line, which will cause scour. By increasing the Reynolds number from 3000 to 7000, the maximum speed in this state increases. The results of the iso pressure lines in Pascals show that the pressure behind the base presses and decreases above and below it. The maximum negative pressure is below the base line of the offshore platform, which will cause scouring. As the Reynolds number increases from 3000 to 7000, the negative pressure in this case increases from -0.07 to -0.3 in Pascal, which will cause scouring. The maximum pressure is below the base line of the offshore platform, which is significantly higher than the case without the use of plates, which reduces the risk of scouring around the base.

1. Introduction

Much research has been done on the investigation of scour around offshore platform baselines, but the main

1,3, 4, MSc
2) Associate Professor
5) MSc student

difference of this research from previous similar cases is the consideration of subsurface slabs under the offshore platform base. Installing impermeable slabs causes the underground flow lines formed under the bed, located under the offshore platform baselines, to be lengthened, as a result of which the pressure gradient across the offshore platform base is reduced. Reducing the pressure gradient is one of the main and most fundamental factors in the formation and development of scour under the offshore platform baselines and the formation of the sluice phenomenon in the bed under the offshore platform baselines. This phenomenon is considered as one of the results of the pressure gradient prevailing over the submerged weight of bed sediment particles.

With the increase in construction in the sea, the use of protective structures to prevent their instability in the marine environment is of interest. Among the coastal protection structures, submerged slabs are used to prevent scour, which are used in marine structural engineering.

There is a hydraulic perspective that studies the distribution of hydrodynamic components around the offshore platform baseline. In fact, this perspective discusses and studies the formation and expansion of eddy currents around the offshore platform baseline through numerical simulations and attempts to accurately estimate the effect of this phenomenon on the amount of hydrodynamic components and the intensity of the effect of eddy formation. Sumer and Fredsoe (1997) studied various environmental conditions (waves and currents) and their effects on the forces acting on the offshore platform baseline. In their research, these researchers often compared their results with the laboratory work of other researchers and confirmed their research based on that. According to the research of these researchers, waves and currents have two completely separate effects on the environment around the offshore platform baseline, the intensity of which can be expressed by the dimensionless Reynolds numbers for the flow and the Cloghan-Carpenter number for the wave. These two dimensionless numbers represent the behavioral properties of the flow and wave, respectively. They also showed that the forces acting on the offshore platform baseline are caused by the effects of environmental conditions in a completely dynamic manner, and the studies conducted by Morrison only calculated the average force acting on the offshore platform baseline. They also introduced the use of the Strouhal number as a suitable method for obtaining the frequency of eddy currents. On the other hand, Cheng and Chew in 2002, using the numerical solution of the fundamental laws of fluids, came up with various hydrodynamic components in the area around the offshore platform baseline. They simulated the conditions of the flow effect in the environment around the offshore platform baseline by formulating and precisely defining the boundary conditions and using the k-4 turbulence model. Cheng and Chew investigated the self-burial effect for unburied offshore platform baselines by adding a rectangular appendage to the offshore platform baseline and comparing the results of the pressure distribution under the new conditions and before adding the appendage. The research of these authors showed that using a numerical model by considering an appropriate turbulence model can easily obtain the amount of various hydrodynamic components around the offshore platform baseline. Liang also stated in his research, which he conducted in collaboration with Cheng in 2004, that the vertical simulation of the flow around the offshore platform baseline using the basic laws of fluids and using one of the types of turbulence modeling methods, is very effective in reducing the cost of studies by various researchers. They confirmed the accuracy of their simulation by comparing their results with the laboratory work done by Jessen (1986). It should be noted that according to Jessen's studies, changing the scale of the problem from the real situation and only considering the ratio of water depth to the diameter of the offshore platform baseline and maintaining the Reynolds number is quite practical and acceptable. In the following, it is necessary to introduce some of the concepts and tools of this division based on which these researchers studied eddy currents.

Reynolds number

This number is used to determine the range of motion of eddies (choi 2000).

$$Re=UD/\upsilon \quad (1)$$

where υ: kinematic viscosity of the fluid, U: flow velocity perpendicular to the offshore platform baseline and D: outer diameter of the offshore platform baseline. Based on the Reynolds number and the observations that researchers made by studying the formation mechanism around the offshore platform baseline, the intensity and formation of vortices can be classified based on the Reynolds number. Among the most important research in this perspective, we can also mention the studies conducted by Sumer Fredose in 1997. These researchers, by dividing the type of fluid space around the offshore platform baseline into two types: permanent and non-permanent

for two different general cases of the presence of the flow effect and the presence of the wave effect, tried to investigate the formation and expansion of vortical flows around the offshore platform baseline resulting from this phenomenon.

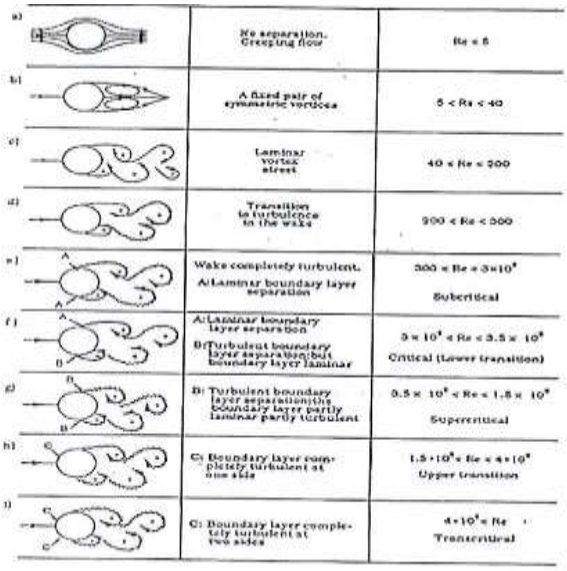

Figure (1): Intensity and formation of vortices based on the Reynolds number (Fredsoe and Sumer in 1997)

shows these different classifications based on the Reynolds number.

As can be seen in Figure (1), for low Reynolds numbers, no separation will be observed behind the offshore platform baseline. In fact, for Zeinolds numbers greater than 5 to 40, a pair of vortices with a fixed shape will be created behind the offshore platform baseline, and the length of the turbulent effect will increase with increasing Reynolds number (Batchelor in 1967). When the Reynolds number of the flow is greater than 40, the shadow of the vortices behind the offshore platform baseline becomes unstable and the turbulence behind the offshore platform baseline is defined by a phenomenon called eddy currents, as a result of which the shadow of the flow appears with eddy lines. When the Reynolds number is in the range (40>Re>200), the eddy lines will appear as layered flows behind the offshore platform baseline. In these cases, the shadow of the eddies is defined as two-dimensional.

With further increase in the Reynolds number, the type of flow behind the offshore platform base changes from a transition flow to a turbulent flow. According to Bloor (1964), when the Reynolds number of the flow is in the range between (200>Re>300) in the area behind the offshore platform base line, the turbulent flow behind the offshore platform base moves towards the offshore platform base line and when the Reynolds number of the flow reaches 400, a turbulent eddy is formed. Observations have shown that a two-dimensional eddy formed in the Reynolds number range (200>Re>40) changes from a two-dimensional state to a three-dimensional state.

The flow with Reynolds number around the offshore platform base line remains completely stratified, and for the flow condition with Reynolds number (3×10^5>Re>40), the flow in the area behind the offshore platform base line is known as the subcritical state. When the flow Reynolds number exceeds this value, the boundary layer state will change from a transitional to a turbulent state. This transition occurs first at the separation point and then moves upstream. For limited flow conditions, when the Reynolds number is in the range (3.5×10^5>Re>3×10^5), the boundary layer at the separation point appears completely turbulent. However, these two states occur only on one side of the offshore platform base and on the other side (the upstream side) it will remain a calm layer. This state is known as the critical flow regime and causes the lift force to be opposite to zero.

When the Reynolds number of the flow reaches 1.5×10^6, the boundary layer on one side of the offshore platform baseline becomes completely turbulent, while on the other side of the offshore platform baseline the flow becomes semi-turbulent. This type of flow regime is known as the upper-transition region, and finally, when the Reynolds number exceeds 4.5×10^6, the boundary layer located on the offshore platform baseline will become completely turbulent at all points.

Mechanism of Vortex Movement

As mentioned, for Reynolds values higher than 40, the boundary layer located on the offshore platform baseline will be separated from the offshore platform baseline due to the unfavorable pressure gradient behind the offshore platform baseline by the formation of a pair of stationary vortices. In this case, a phenomenon as shown in Figure (2) will be formed behind the offshore platform baseline. As can be seen in Figure (2), the boundary layer formed around the offshore platform baseline has characteristic values of local vorticity.

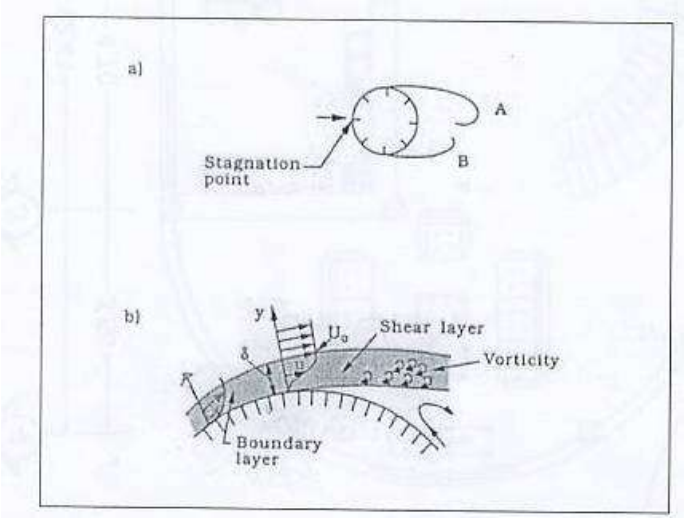

Figure (2): Location of the separation point in front of the offshore platform baseline and the development of the shear layer behind the offshore platform baseline.

These vortices are formed within the boundary layer, develop, and cause rotation of a vorticity with a specific shape above and below the offshore platform baseline.

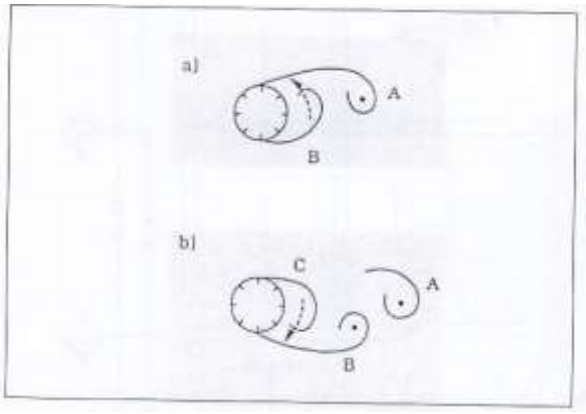

Figure (3): How vortical flows develop behind the offshore platform baseline
(Gerrard in 1966)

In fact, the motion of vortices is unstable for flow Reynolds numbers greater than 40, and the direction and manner of motion of vortices can be justified based on the opinion of Gerrard in 1966. Based on Figure (3), he assumed that vortex A starts earlier than vortex B and the direction of vortex formation is opposite to each other. If vortex A is expanding clockwise and vortex B is expanding counterclockwise, vortex B will cause vortex A to break away from the boundary layer and vortex A will separate and move downstream as a free vortex. This expansion will then produce vortex C and similarly, in the opposite direction, will cause vortex B to separate from its source of generation. This process will be repeated periodically over time behind the offshore platform baseline.

In fact, the motion of vortices is unstable for flow Reynolds numbers greater than 40, and the direction and manner of motion of vortices can be justified based on the opinion of Gerrard in 1966. Based on Figure (3), he assumed that vortex A starts earlier than vortex B and the direction of vortex formation is opposite to each other. If vortex A is expanding clockwise and vortex B is expanding counterclockwise, vortex B will cause vortex A to break away from the boundary layer and vortex A will separate and move downstream as a free vortex. This expansion will then produce vortex C and similarly, in the opposite direction, will cause vortex B to separate from its source of generation. This process will be repeated periodically over time behind the offshore platform baseline. The motion of water particles in a wave is a continuous unsteady flow. When this unsteady flow collides with a rigid body of a submerged structure, a force is exerted on the body due to the flow velocity and the flow acceleration.

The flow velocity creates a drag force Fd that acts on the body of the submerged structure and is due to the frictional shear stress and the total pressure, which is usually calculated by the following formula:

$$F_d = \frac{C_d}{2}\rho A u^2 \quad (2)$$

A is the distance of the cross section perpendicular to the flow surface. In equation (2) u is the flow velocity reaching the body, ρ is the density of the liquid, cd is the drag coefficient that depends on the cross section shape, flow direction, surface roughness and the Reynolds number of the flow.

For a cylinder, the Reynolds number is R=UD/υ, where D is the diameter of the cylinder and υ is the kinematic viscosity of the flow.

When a flow is accelerated over a surface, the flow velocity and hence the Reynolds number and, in some cases, the continuous elastic coefficient change. Therefore, since u and Cd are both variable in an accelerated flow, the elastic force of equation (2) can change considerably.

The acceleration of the flow produces an additional force on the body, in addition to that given in equation (2). This acceleration or inertial force has two components. The first component is due to the acceleration of the flow due to the pressure difference in the accelerating flow field. This pressure difference creates a variable pressure on the surface of the body of the body, which creates a net force on the body. Also, when an accelerated flow passes over a body, an additional mass of fluid is created due to the presence of the body in motion. When the flow passing over a stationary surface is accelerated, there will be an additional mass that creates a force on the body. This second component is related to the inertial force, a function of the density and acceleration of the fluid, as well as the shape of the object and its volume.

Therefore, when there is an unsteady flow, the total instantaneous hydrodynamic force F on the object can be written as:

$$F = \frac{C_d}{2}\rho A u^2 + \int_A P_x dA + K\rho V \frac{du}{dt} \quad (3)$$

The second term on the right, where Px is the pressure exerted on the body of the object in the direction of the flow and dA is the change in the area of the place where the pressure is exerted, is the inertial force due to the acceleration of the pressure difference of the flow field. The third term on the right is the added mass (Khosro Bargi).

In the present study, first the effect of offshore platform baselines with their different diameters on the scouring process is investigated; then by installing an impermeable subgrade sheet in front of the offshore platform baselines, the effect of this sheet on the scouring phenomenon is studied.

In this study, the flow simulation after the construction of the submerged sheet was investigated using the computational fluid dynamics method and Fluent software.

2. Methods

A critical review of available turbulence models with the aim of evaluating their suitability for use in hydraulic problems is valuable and needed. This

was done by Professor Wolfgang Reddy with years of experience in the development and application of these models. In the book ((turbulence models and their application in hydraulics)), he introduced the topic of turbulence modeling in a simple way that can be understood by any reader with basic knowledge in the field of fluid mechanics and summarized the latest published articles in this field. is In the first chapter, the role of turbulence models is explained (Salehi Nishabouri and Nasiri Saleh, 2017).

Basic conservation laws are expressed by exact equations (Navier-Stokes equations). They describe all the details of fluid movement. Since there is little hope to solve these equations and also due to the lack of interest of engineers in the details of oscillatory motion, a statistical approximation (which was first proposed by Asburn Reynolds) was used and these equations, on the time scale - which in The comparison with the time scale of turbulent motion is large - they were averaged.

Unfortunately, the averaging operation creates a new problem that the equations cannot form a closed system, because they contain unknown sentences that describe the transfer of the amount of motion, heat, and average mass by means of turbulent motion. This system of equations can be closed only by using experimental input, therefore, calculation methods based on averaged flow equations are semi-empirical.

The so-called field methods - which use the original partial differential equations - require the specifications of the turbulent transfer terms that appear in the equations at every point of the flow. This specification is defined by using the equations (algebraic or differential) that determine the turbulent transfer terms in the average flow equations, and the system of equations is closed using those equations. The basis of chaos models are hypotheses about chaotic processes that require experimental input in the form of constants or functions. They do not simulate the details of the turbulent motion, but simply "simulate the effect of turbulence on the behavior of the average flow" (Salehi Nishabouri and Nasiri Saleh, 2017).

In this study, flow is unsteady with two-dimensional turbulence form. Velocity and pressure are a function of time and space. To model of the velocity and pressure fluctuations is the integrated from the Navier Stokes equation at time. Integration of Navier Stokes equations at time is known Reynolds equations (Reynolds, 1984). Turbulence model equations are two equation models k-ε (Standard) that have be averaged in depth (Rastogi and Reddy, 1978). ε equation is as one of the main sources of the limitations of accuracy of the standard version of the k-ε model and the Reynolds stress model. It is interesting that k-ε model includes a correction term that is dependent to strain with c13 constant in the ε equation of RNG model (Yakhot et al, 1992). WillCox provided turbulence equations of k-ω (standard) model (WillCox, 1988).

$$\frac{\partial u}{\partial x}+\frac{\partial v}{\partial y}+\frac{\partial w}{\partial z}=0$$

(4)

$$\frac{\partial \rho u}{\partial t}+\frac{\partial \rho uu}{\partial x}+\frac{\partial \rho uv}{\partial y}+\frac{\partial \rho uw}{\partial z}-\rho f_c v=-\frac{\partial P}{\partial x}+\frac{\partial \tau_{xx}}{\partial x}+\frac{\partial \tau_{xy}}{\partial y}+\frac{\partial \tau}{\partial z}$$

(5)

$$\frac{\partial \rho v}{\partial t}+\frac{\partial \rho uv}{\partial x}+\frac{\partial \rho vv}{\partial y}+\frac{\partial \rho vw}{\partial z}+\rho f_c u=-\frac{\partial P}{\partial y}+\frac{\partial \tau_{yx}}{\partial x}+\frac{\partial \tau_{yy}}{\partial y}+\frac{\partial \tau_{y}}{\partial z}$$

(6)

$$\frac{\partial \rho w}{\partial t}+\frac{\partial \rho uw}{\partial x}+\frac{\partial \rho vw}{\partial y}+\frac{\partial \rho ww}{\partial z}=-\frac{\partial P}{\partial z}+\frac{\partial \tau_{zx}}{\partial x}+\frac{\partial \tau_{zy}}{\partial y}+\frac{\partial \tau_{zz}}{\partial z}-\rho g$$

(7)

Turbulence model equation

Known two-equation model of k-ε (Standard) are presented for averaged form in depth as follows: (Rastogi and Reddy, 1978).

$$\frac{\partial hk}{\partial t}+\frac{\partial U_j hk}{\partial x_j}=\frac{\partial}{\partial x_j}[(\nu+\frac{\nu_t}{\sigma_k})h\frac{\partial k}{\partial x}]+hP_k+hP_{kv}-h\varepsilon \quad (8)$$

$$\frac{\partial h\varepsilon}{\partial t}+\frac{\partial U_j h\varepsilon}{\partial x_j}=\frac{\partial}{\partial x_j}[(\nu+\frac{\nu_t}{\sigma\varepsilon})h\frac{\partial \varepsilon}{\partial x}]+hc_{1\varepsilon}\frac{\varepsilon}{k}P_k+hP_{\varepsilon v}-hc_{2\varepsilon}\frac{\varepsilon^2}{k}$$

(9) $$\frac{\partial h\varepsilon}{\partial t}+\frac{\partial U_j h\varepsilon}{\partial x_j}=\frac{\partial}{\partial x_j}\left[\left(\nu+\frac{\nu_t}{\sigma_\varepsilon}\right)h\frac{\partial \varepsilon}{\partial x}\right]+hc_{1\varepsilon}\frac{\varepsilon}{k}P_k+hP_{\varepsilon v}-hc_{2\varepsilon}\frac{\varepsilon^2}{k}$$

$$\nu_t=c_\mu\frac{k^2}{\varepsilon},P_k=2\nu_t S_{ij}.S_{ij} \quad (10)$$

$$P_{kv}=c_k\frac{k^2}{\varepsilon},c_k=\frac{1}{c_f^{1/2}},P_{\varepsilon v}=c_\varepsilon\frac{u_f^4}{h^2},c_\varepsilon=\frac{1}{\sqrt{e_*\sigma_t}}\frac{c_{2\varepsilon}c_\mu^{1/2}}{c_f^{3/4}},c_f=\frac{u_f^2}{u^2+v^2+w^2}=\frac{n^2g}{h^{1/3}} \quad (11)$$

$$c_\mu=0.09,c_{\varepsilon1}=1.44,c_{\varepsilon2}=1.92,\sigma_k=1.0,\sigma_\varepsilon=1.31$$

P_{kv} and P_{kv} are production terms as result of non-uniform distribution velocity in depth that is stronger near-bed. P_k is production term of turbulent kinetic energy averaged in depth as result of velocity gradients in the plan. ν_t is the vortex viscosity. Turbulence model is used for calculation of lateral flow into one channel and is achieved much better results in comparison with ν_t for fixed parameters of rotational flow (MCGurik and Rodi, 1978). c_f is the bed friction coefficient. σ_t is Schmidt number that shows relationship between turbulence viscosity and turbulent diffusion coefficient according to the following equation:

$$\varepsilon_d=\frac{\nu_t}{\sigma_t} \quad (12)$$

Amount of σ_t is considered 0.5 (Keller and Rodi, 1988). Although values of σ_t are 0.5 to 2 in variable references (Gibson and launder, 1978). e_* is coefficient that gives turbulence diffusion coefficient in depth by following equation (Keller and Rodi, 1988).

$$\varepsilon_d=e_*hu_f \quad (13)$$

Direct measurement of color broadcasting in the fixed-width channels offers 0.15 for e_*. Although Keller and Rodi achieved better solutions for the velocity and stress within the composite channels (Keller and Rodi, 1988). On the other hand Biglari and Sturm have been assumed e_* equaled to 0.3 to get the better answer within the composite channels (Biglari and Sturm, 1998). MCGurik and Rodi have considered $\frac{1}{\sqrt{e_*\sigma_t}}$

equaled to 3.6 (MCGurik and Rodi, 1978). In ε equation of RNG model includes a correction term $c_{\varepsilon 1}$ that is *constant strain-dependent (Yakhot et al, 1992). For k-ε (RNG), we have:*

$$\frac{\partial h\varepsilon}{\partial t}+\frac{\partial U_j h\varepsilon}{\partial x_j}=\frac{\partial}{\partial x_j}[(\nu+\frac{\nu_t}{\sigma\varepsilon})h\frac{\partial\varepsilon}{\partial x}]+hc^*_{1\varepsilon}\frac{\varepsilon}{k}P_k+hP_{\varepsilon\nu}-hc_{2\varepsilon}\frac{\varepsilon^2}{k} \quad (14)$$

$$c_\mu=0.0845, c^*_{1\varepsilon}=c_{1\varepsilon}-\frac{\eta(1-\frac{\eta}{\eta_0})}{1+\beta\eta^3}, c_{1\varepsilon}=1.68, \sigma_k=1.39, \beta=0.012, c_{1\varepsilon}=1.42,$$

$$\eta=(2E_{ij}.E_{ij})^{1/2}\frac{k}{\varepsilon}, \eta_0=4.377 \quad (15)$$

Only constant β is adjustable, high levels of turbulent data are obtained near-wall. All other constants are calculated explicitly as part of the RNG process.

$$\frac{\partial hk}{\partial t}+\frac{\partial U_j hk}{\partial x_j}=\frac{\partial}{\partial x_j}[(\nu+\frac{\nu_t}{\sigma_k})h\frac{\partial k}{\partial x}]+P_k+P_b-h\varepsilon \quad (16)$$

$$\frac{\partial h\varepsilon}{\partial t}+\frac{\partial U_j h\varepsilon}{\partial x_j}=\frac{\partial}{\partial x_j}[(\nu+\frac{\nu_t}{\sigma\varepsilon})h\frac{\partial\varepsilon}{\partial x}]+hc_{1\varepsilon}\frac{\varepsilon}{k}P_k+hc_1S_\varepsilon-hc_2\frac{\varepsilon^2}{k+\sqrt{\nu\varepsilon}}+S_\varepsilon \quad (17)$$

$$c_1=Max[0.43,\frac{\eta}{\eta+s}], \eta=s\frac{k}{\varepsilon}, s=\sqrt{2s_{ij}s_{ij}}, \mu_t=hc_\mu\frac{k^2}{\varepsilon}, P_k=-\rho\overline{u_i^{'}u_j^{'}}\frac{\partial u_j}{\partial x_i^{'}},$$

$$P_k=\mu_t s^2, P_b=\beta g_i\frac{\mu_t}{\Pr_t}\frac{\partial T}{\partial x_i}, \mu_t=\rho c_\mu\frac{k^2}{\varepsilon}, c_\mu=\frac{1}{A_0+A_s\frac{KU^*}{\varepsilon}}, U^*=\sqrt{s_{ij}s_{ij}+\overline{\Omega_{ij}}\,\overline{\Omega_{ij}}}, \quad (18)$$

$$\overline{\Omega_{ij}}=\Omega_{ij}-\varepsilon_{ijk}\omega_k, A_0=4.04, A_s=\sqrt{6}\cos\Phi, \Phi=\frac{1}{3}\cos^{-1}(\sqrt{6}\omega), \omega=\frac{s_{ij}s_{jk}s_{ki}}{\tilde{s}^3}, \tilde{s}=\sqrt{s_{ij}s_{ij}},$$

$$s_{ij}=\frac{1}{2}(\frac{\partial u_j}{\partial x_i}+\frac{\partial u_i}{\partial x_j}), c_{1\varepsilon}=1.44, c_2=1.9, \sigma_k=1, \sigma_\varepsilon=1.2, \beta=-\frac{1}{\rho}(\frac{\partial P}{\partial T})p, \Pr_t=0.85$$

WillCox, turbulence model k-ω (standard) equation to be provided as follows: (WillCox, 1988):

$$\frac{\partial k}{\partial t}+U_j\frac{\partial k}{\partial x_j}=\tau_{ij}\frac{\partial U_i}{\partial x_j}-\beta^*k\omega+\frac{\partial}{\partial x_j}[(\nu+\sigma^*\nu_T)\frac{\partial k}{\partial x_j}] \quad (19)$$

$$\frac{\partial\omega}{\partial t}+U_j\frac{\partial\omega}{\partial x_j}=\alpha\frac{\omega}{k}\tau_{ij}\frac{\partial U_i}{\partial x_j}-\beta\omega^2k\omega+\frac{\partial}{\partial x_j}[(\nu+\sigma\nu_T)\frac{\partial\omega}{\partial x_j}] \quad (20)$$

$$\frac{\partial k}{\partial t}+U_j\frac{\partial k}{\partial x_j}=\tau_{ij}\frac{\partial U_i}{\partial x_j}-\beta^*k\omega+\frac{\partial}{\partial x_j}[(\nu+\sigma^*\nu_T)\frac{\partial k}{\partial x_j}] \; \nu_t=\frac{k}{\omega}, \alpha=\frac{5}{9}, \beta=\frac{3}{40}, \beta^*=\frac{9}{100}, \sigma=\frac{1}{2}, \varepsilon=\beta^*\omega k$$

3. Result and discussions

The values of the physical properties of water are considered as a default respectively, for density, viscosity, heat capacity and thermal conductivity. Solutions of all governing equations are subject to assignment of variables correctly in the boundary nodes. In steady state problems required only boundary condition but in unsteady state problems is required the initial conditions for all nodes in the network. Common boundary conditions in hydraulic issues include (Soltani and Rahimi Asl, 2003):

A- Inlet boundary condition: numerical models can fit the model by means of the various boundary conditions such as velocity, mass flow, etc. For example, in modeling of flow inside a closed or open channel can be used velocity inlet as input boundary condition.

B- The outlet boundary condition is considered pressure outlet equals the atmospheric pressure. If the output is chosen at a far distance from geometric constraints, and no change in direction of flow then the flow state is developed full. Using this model is caused the output surface is perpendicular to the flow and gradient is zero in the perpendicular direction on the output surface (Soltani and Rahimi Asl, 2003).

C - Wall boundary condition: the wall boundary condition is used to limit the area of between fluid and solid. The model is ready for simulation by Solutions set and defining the model. The following steps show the simulation process (Versteeg and Malalasekera, 2007): selection methods of discretization equation: In this paper first order upstream difference method is used for discretization of momentum, k, ε and ω equations and the standard method is used to find the pressure. Selection methods of the relation velocity - Pressure: this step is only be studied segregated. In this paper is used from SIMPLE method for velocity - pressure coupling. Determine the discount factors: the discount factor values are used for control of calculated variables in the each iteration. In this paper, the default values are used respectively for the pressure, density, momentum, k, ε and turbulent viscosity. In this paper, the initial values of the relative pressure is considered zero And the initial values of velocity components close to the average values presented in the input stream. By completing the steps in the numerical model, we can start the introduced process of problem by defining of repeat process. The frequency of reporting of results can be introduced before computing the numerical model. During solution process can be seen convergence of solution by the control of residues, integral of surface, statistics and values of the force. After finishing solution the computation of the unknown quantities and the results can be calculated at any point of the field and can be displayed by vector in the form, contour and profile views (Versteeg and Malalasekera, 2007). In this paper for solution of flow is usually introduced initial number repeat 1000 with report of every step of the calculation that conditions for convergence of the unknown parameters were satisfied after 300 to 350 iterations.

5. Discussion

In this research, Gambit software version 16.3.2 has been used to generate the geometry and mesh it. The mesh pattern is Quad element and map type is used for the surfaces. The existing boundary conditions are velocity input from the left side from the top of the arc and pressure output boundary condition at the bottom of the arc outlet. The simulation results are seen in Figures 5 to 21.

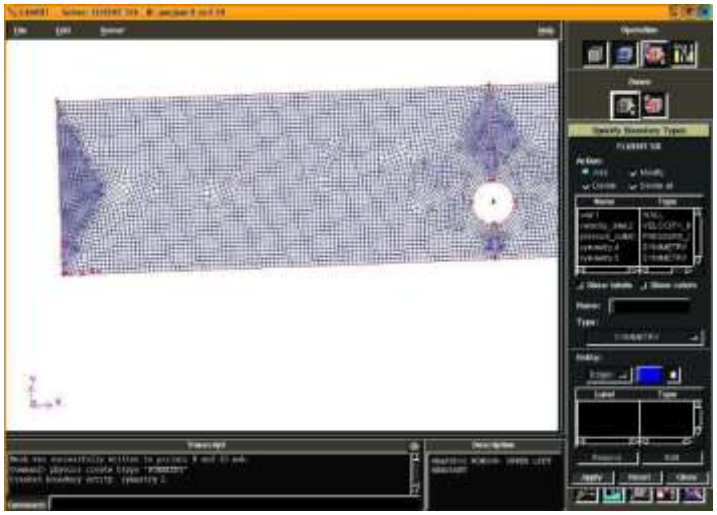

Figure 5 - Model geometry in Gambit software

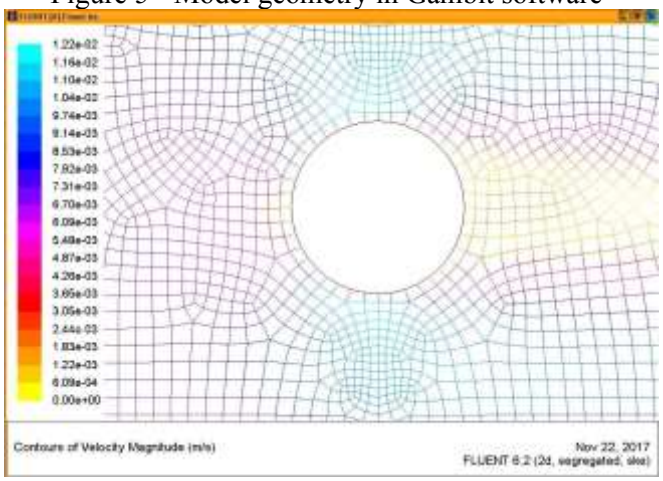

Figure 6 - The velocity curve, m/s, shows that the velocity values decrease behind the offshore platform base. The maximum velocity value is below the offshore platform base line, which will cause scour.

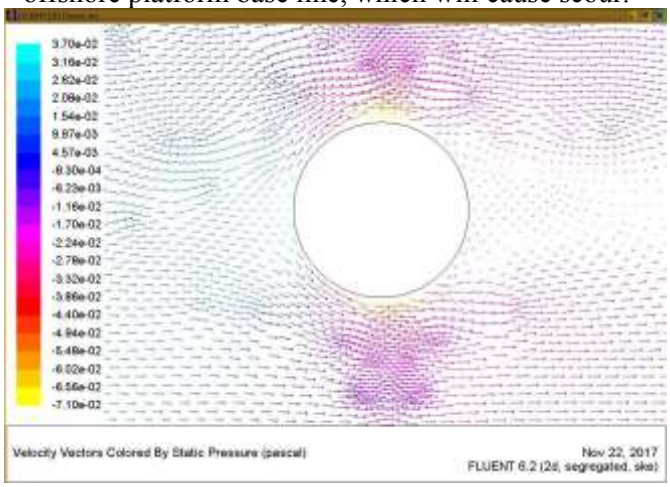

Figure 7 - The iso pressure in Pascals show that the pressure values decrease behind the offshore platform base and above and below it. The maximum negative pressure is below the offshore platform base line, which will cause scour.

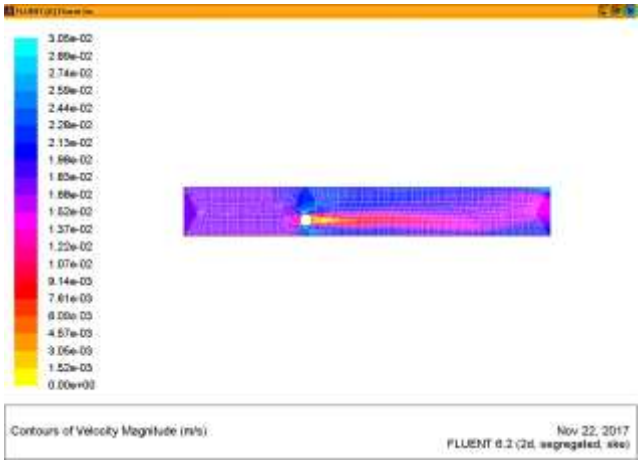

Figure 8- Lines of constant velocity, m/s, results show that the velocity values decrease behind the offshore platform base. The maximum velocity value is below the offshore platform base line, which will cause scour.

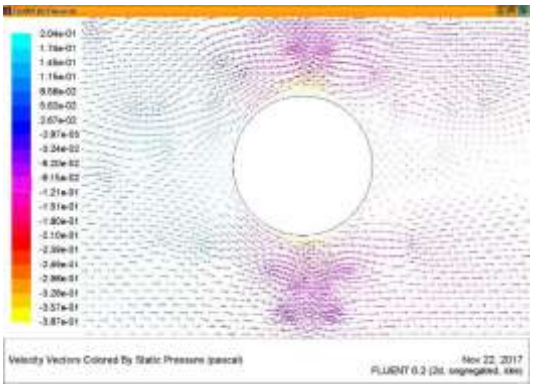

Figure 9- Iso pressure lines in Pascal, the results show that the pressure values behind the offshore platform base and above and below it decrease. The maximum negative pressure value is below the offshore platform base line, which will cause scouring. By increasing the Reynolds number from 3000 to 7000, the negative pressure value in this case increases.

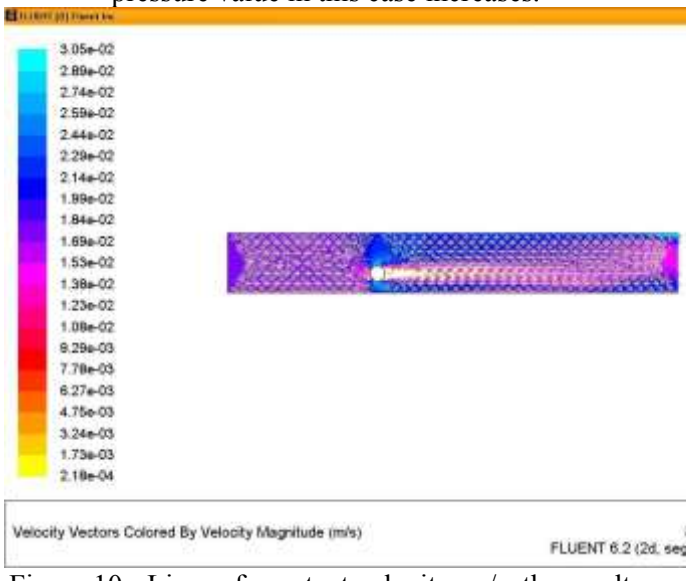

Figure 10 - Lines of constant velocity, m/s, the results show that the velocity values decrease behind the offshore platform base. The maximum velocity value is below the offshore platform base line, which will cause scour. By increasing the Reynolds number from 3000 to 7000, the maximum velocity value in this case increases.

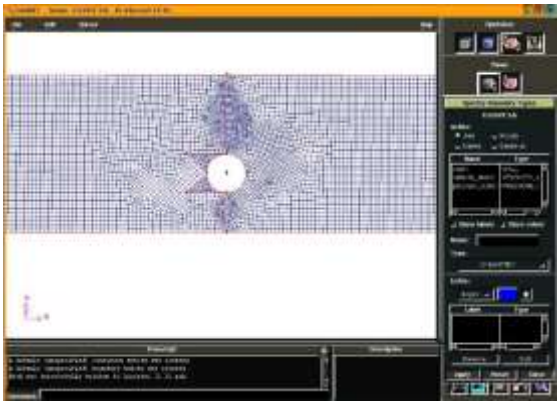

Figure 11 - Meshing and geometry of the model created for the impact of barrier plates in front of the offshore platform base.

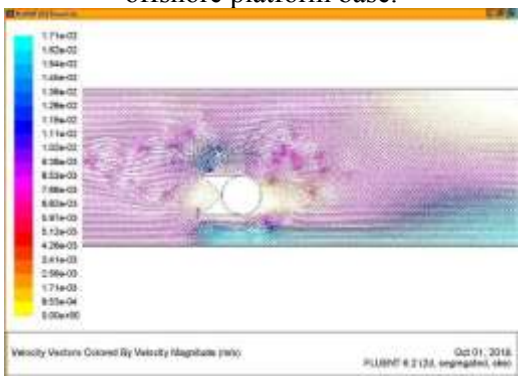

Figure 12 - Lines of constant velocity, m/s, results show that the velocity values decrease behind the offshore platform base. The maximum velocity value is below the offshore platform base line, which will cause scouring at a distance further from the base due to the presence of barrier plates.

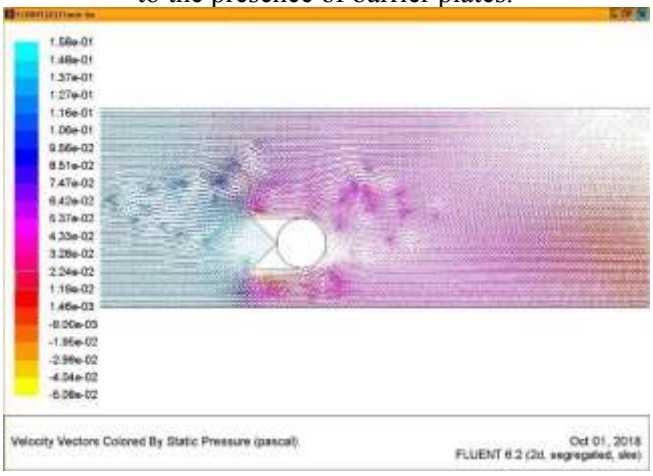

Figure 13- Isobaric lines in Pascal, the results show that the pressure values behind the offshore platform base and above and below it decrease. The maximum negative pressure value is below the offshore platform base line, which is significantly reduced compared to the case without the use of barrier plates.

4. Conclusion

The reduction of the pressure gradient is one of the most important and fundamental factors in the formation and development of scour around the base of an offshore platform and the formation of the sluice phenomenon in the bed around the base of the offshore platform. This phenomenon is considered as one of the results of the pressure gradient prevailing over the submerged weight of bed sediment particles.

In the present study, the effect of the offshore platform base lines with their different diameters on the scour process is first investigated; then, by installing an impermeable sheet in front of the offshore platform base lines, the effect of this sheet on the scour phenomenon is studied.

Laboratory results indicate that the use of impermeable sheets in front of the offshore platform base lines to some extent prevents the formation of scour tunnels around the offshore platform base lines and protects them from the dangers caused by scour.

In this study, the simulation of the flow around the submerged offshore platform base with different Reynolds number states was investigated using the computational fluid dynamics method and Fluent software.

The results of the first model for the isovelocity lines, m/s, show that the velocity values behind the offshore platform base decrease from 0.006 to 0.00006.

The maximum velocity value is below the offshore platform base line, which will cause scouring. By increasing the Reynolds number from 3000 to 7000, the maximum velocity value increases in this case.

The results of the isopressure lines in Pascals show that the pressure values behind the offshore platform base and above and below it decrease. The maximum negative pressure value is below the offshore platform base line, which will cause scouring. By increasing the Reynolds number from 3000 to 7000, the negative pressure value in this case increases from minus 0.07 to minus 0.3 in Pascals, which will cause scouring. The maximum negative pressure value is below the offshore platform base line, which is significantly reduced compared to the case without the use of barrier plates.

5. References

1. Sorenson Robert M. - 1938 - Principles of Marine Engineering - Khosrow Bargi - Tehran University Publications Institute.
2. [1]Fredsoe, J., E. A. Hansen, Ye Mao, and B. M. Sumer. "Three-dimensional scour below pipelines." Journal of Offshore Mechanics and Arctic Engineering110, no. 4 . 373-379, 1988.
3. Chiew, Yee-Meng. "Mechanics of local scour around submarine pipelines."Journal of Hydraulic Engineering 116, no. 4. 515-529, 1990. [3] Sumer, B. Mutlu, and Jørgen Fredsøe. "Scour around pipelines in combined waves and current ". No. CONF-9606279--. American Society of Mechanical Engineers, New York, NY (United States), 1996.
4. Yang, Bing, Fu-Ping Gao, Dong-Sheng Jeng, and Ying-Xiang Wu. "Experimental study of vortexinduced vibrations of a pipeline near an erodible sandy seabed." Ocean engineering 35, no. 3.301-309, 2008.
5. Gao, Fu-Ping, Bing Yang, Ying-Xiang Wu, and Shu-Ming Yan. "Steady current induced seabed scour around a vibrating pipeline." Applied Ocean Research 28, no. 5.291-298, 2006.
6. Zhao, Ming, and Liang Cheng. "Numerical investigation of local scour below a vibrating pipeline under steady currents." Coastal Engineering 57, no. 4 .397-406, 2010.
7. Zhou, Chunyan, Guangxue Li, Ping Dong, Jinghao Shi, and Jishang Xu. "An experimental study of seabed responses around a marine pipeline under wave and current conditions." Ocean Engineering 38, no. 1 .226-234, 2011.
8. Yang, Lipeng, Bing Shi, Yakun Guo, Lixiang Zhang, Jisheng Zhang, and Yan Han. "Scour protection of submarine pipelines using rubber plates underneath the pipes." Ocean Engineering 84 .176-182, 2014.
9. Yang, Lipeng, Bing Shi, Yakun Guo, and Xianyun Wen. "Calculation and experiment on scour depth for submarine pipeline with a spoiler." Ocean Engineering 55 .191-198, 2012.
10. Sumer, B. M., and J. Fredsoe. "Onset of scour below a pipeline exposed to waves." In The First International Offshore and Polar Engineering Conference. International Society of Offshore and Polar Engineers, 1991.
11. Li, Fangjun, and Liang Cheng. "Prediction of lee-wake scouring of pipelines in currents." Journal of waterway, port, coastal, and ocean engineering (2001).
12. Sumer, B. Mutlu, Christoffer Truelsen, T. Sichmann, and Jørgen Fredsøe. "Onset of scour below pipelines and self-burial." Coastal engineering 42, no. 4 .313-335, 2001.
13. *Reynolds, O., 1984. On the dynamical theory of incompressible viscous fluids and the determination of the criterion. Phil. Trans. Roy. Soc. London, 123-161.*
14. *McGurik, J.J. and Rodi, W., 1978. A depth-averaged mathematical model for the near fluid of side discharge into open- channel flow. Journal of Fluid Mechanics, 864, 761-781.*
15. *Keller, R.J. and Rodi, W., 1988. Prediction of flow characteristics in main channel/floodplain flows. Journal of Hydraulic Research, IAHR, 26(4), 425- 441.*

16. *Biglari, B. and Sturm, T.W., 1998. Numerical modeling of flow around bridge abutments in compound channel. Journal of Hydraulic Engineering, ASCE, 124(2), 156-163.*
17. *Gibson, M.M. and Launder, B.E., 1978. Ground effects on pressure fluctuations in the atmospheric boundary layers. Journal of Fluid Mechanics, 86, 491-511.*
18. *Rastogi A. K. and Rodi, W., 1978. Prediction of heat and mass transfer in open channels. Journal of Hydraulics Division, ASCE, 104(3), 397- 420.*
19. *Yakhot V., Orszag S.A., Thangam, S., Gatski, T.B. and speziale, C.G., 1992. Development of turbulence models for shear flows by a double expansion technique. Physics of Fluids A, Vol. 4, No. 7, pp1510-1520.*
20. *Wilcox D.C., 1988. Re-assessment of the scale-determining equation for advanced turbulence models. AIAA Journal, vol. 26, pp. 1414- 1421.*
21. *Versteeg, H.K. and Malalasekera, W., 2007. An Introduction to Computational Fluid Dynamics: The Finite Volume Method, Prentice Hall, Feb 16, 503 pages.*
22. *Soltani, M.V. and Rahimi Asl, R., 2003. Computational fluid dynamics by Fluent software, Tehran, Tarrah issues.*